Observation of the marine atmospheric boundary layer in the Gulf of Guinea during the 2006 boreal spring

Marion Leduc-Leballeur, Laurence Eymard, Gaëlle de Coëtlogon

Observation of the marine atmospheric boundary layer in the Gulf of Guinea during the 2006 boreal spring

Marion Leduc-Leballeur,[a] Laurence Eymard[b] and Gaëlle de Coëtlogon[a]*
[a]*LATMOS–IPSL, UPMC, Paris, France*
[b]*LOCEAN–IPSL, UPMC, Paris, France*

***In situ*, satellite and model analyses data in April–July 2006 are used to investigate the links between sea surface temperature (SST) and the marine atmospheric boundary layer (MABL) in the Gulf of Guinea. The study region between 10°W and 6°E is divided into three areas with different characteristics: the North Area (4.5°N to 1°N) with the wettest atmosphere and the warmest SST, the Upwelling Area (1°N to 4°S) with the strongest SST decrease, and the South Area (4°S to 8°S) with a drier atmosphere and a more slowly decreasing SST than in the Upwelling Area. The key zone of the air-sea interactions in this region seems to be the SST front between North and Upwelling Areas. On the one hand, the study of the MABL on either side of the front shows a well-mixed layer between the surface and about 500 m high, sensitive to surface variations, which gets shallower (deeper) when the SST decreases (increases). The MABL height (about 1500 m) follows the same variations but is not exactly collocated with the SST variations. On the other hand, the observation of the MABL across the SST front shows a strengthening of southeasterlies in the South Area coinciding with a strong SST decrease in the Upwelling Area. In the latter, the wind weakens above the colder SST. Besides, in the North Area, the wind strengthens above the warmer SST. However, the wind acceleration spans from the equator to 2°N in April and as far as 4°N in June. A convergence zone is observed in the vicinity of 2°N in April, suggesting a convection activity there, favoured by the SST front.**

Key Words: boundary layer; air-sea interaction; tropical Atlantic

Received 20 June 2010; Revised 26 November 2010; Accepted 1 February 2011

Citation: Leduc-Leballeur M, Eymard L, de Coëtlogon G. 2011. Observation of the marine atmospheric boundary layer in the Gulf of Guinea during the 2006 boreal spring. Q. J. R. Meteorol. Soc. 137: 992–1003. doi:10.1002/qj.808

1. Introduction

In the Gulf of Guinea, an equatorial upwelling develops in boreal summer (Merle *et al.* 1980; Picaut 1983). At the same time, the West African monsoon is engaged by an abrupt latitudinal shift of the intertropical convergence zone (ITCZ) from about 5°N in May–June to about 10°N in July–August (Sultan and Janicot 2003). Caniaux *et al.* (2011) observed a high correlation between the onset of the equatorial upwelling and this northward jump of the ITCZ. Several authors suggested an influence of the sea surface temperature (SST) cooling on the West African monsoon onset (Vizy and Cook 2001, 2002; Sultan and Janicot 2003; Gu and Adler 2004; Okumura and Xie 2004). However, the mechanisms of this influence are still largely unknown.

To provide a better understanding of the processes playing a role in the West African monsoon, the African Monsoon Multidisciplinary Analysis (AMMA) programme (Redelsperger *et al.* 2006) performed an extensive observation period between 2005 and 2007, with an intensive field campaign in 2006 (Janicot *et al.* 2008). Thanks to this programme, the oceanic mixed layer and upwelling processes are better known (Marin *et al.* 2009; Caniaux *et al.* 2011; Wade *et al.* 2010), as well as the oceanic circulation there (Kolodziejczyk *et al.* 2009). However, the marine atmospheric boundary layer (MABL) processes remain poorly documented. In particular, interactions between the SST and the MABL need an exhaustive study

in order to understand how the upwelling and the resulting colder SST impact the humidity transport, which comes and supplies the West African monsoon.

Between April and July, the whole eastern equatorial Atlantic is cooling. However, the cooling in the equatorial upwelling is faster and creates a strong SST gradient between the cold water south of the equator and the warmer one north of 1°N. Conversely, the SST gradient at its southern boundary is weak, as the SST is colder south of the upwelling than north of 1°N (Figure 1 (a)). Several previous experiments were conducted in the Pacific and North Atlantic oceans in the vicinity of such SST gradients, such as the Joint Air–Sea Interaction (JASIN; Pollard *et al.* (1983)), the Frontal Air–Sea Interaction Experiment (FASINEX; Stage and Weller (1985)) and the "Structure des Echanges Mer–Atmosphère, Propriétés des Hétérogénéités Océaniques: Recherche Expérimentale" (SEMAPHORE; Eymard *et al.* (1996)). For a wind blowing from cold to warm SST, a strengthening of the wind, an increase of the turbulent fluxes and a thickening of the MABL above the warm side of the SST front were mainly observed (Businger and Shaw 1984; Friehe *et al.* 1991; Kwon *et al.* 1998). These characteristics now need to be studied in the frontal zone in the Gulf of Guinea.

The aim of this study is to explore the MABL characteristics and investigate the possible links between the cooling of the SST leading the development of the front, and the MABL in the Gulf of Guinea during the 2006 season, using in situ and satellite data, as well as model analyses. A focus is made at the time of the equatorial upwelling formation, between April and July 2006. Section 2 describes the data used for the study. General characteristics of the eastern equatorial Atlantic are exposed in section 3, followed by a description of the observed effects of the SST on the MABL, on either side and across the SST front, in section 4. Finally, the results are discussed in section 5.

2. Data

All the data described below were supplied by the AMMA database (http://database.amma-international.org/; Fleury *et al.* (2011)).

2.1. In situ data

Within the oceanic component "Etude de la circulation océanique et du climat dans le golfe de Guinée" (EGEE) of the AMMA programme, an oceanic survey of the Gulf of Guinea was made in May–July 2006 (EGEE–3) (Bourlès *et al.* 2007). The covered region is located between 5°N–10°S and 10°W–10°E (Figure 1). During the cruise, air temperature, SST, relative humidity and wind were continuously measured, as well as the total column water vapour (WV). Radiosoundings measuring air temperature, relative humidity, pressure and wind were launched two to four times a day.

2.2. Satellite measurements

Satellite measurements were used to supplement and put the EGEE–3 survey into a regional perspective. Specifically, the TRMM Microwave Imager (TMI) measures the SST through clouds, except under rainy conditions, and the WV (Wentz 1997; Wentz *et al.* 2000). In addition, the QuikScat (Quick Scatterometer) satellite provided wind vector data (Liu *et al.* 2000). These satellite data are available as 3–day running mean on a 0.25° grid.

2.3. ECMWF operational analyses

The operational analyses from the European Centre from Medium–Range Weather Forecasts (ECMWF) provide surface parameters (air temperature, SST, WV and wind) and atmospheric profiles (air temperature, specific humidity and wind). In contrast to the satellite data, they allow the study of the low atmosphere vertical structure. The horizontal resolution is 0.25° from April to July 2006 with 6–hourly data (0, 6, 12 and 18 h). The 91 model levels provide a good vertical precision for the boundary layer study, with 20 levels between the surface and about 3000 m. However, the available dataset on the AMMA database is limited to 5°S in latitude.

2.4. Consistency analysis of the datasets

Figure 2 shows the hourly mean of the SST and WV measured along the cruise compared to the closest satellite and model data in time and space. The mean and standard deviation (STD) are very similar for the three SST datasets (Table 1). However, if the mean differences between cruise measurements, satellite and ECMWF SST data are very small, some important differences exist punctually (STD of about 0.5°C). The same goes for the WV, where the most important differences are observed near the African coast (about 10 kg m^{-2} during 15–25 June and the first days of July), where the rainfall perturbs the sensor. Note that the EGEE–3 cruise radiosoundings and QuikScat wind measurements are assimilated in the ECMWF operational analyses.

3. Overview of April–July 2006

Figure 1(a), which shows the TMI SST mean map from 15 May to 15 June 2006, suggests a zonal pattern of the SST in the eastern equatorial Atlantic, and similarly for TMI WV and QuikScat wind speed (not shown). Roughly, three different regions appear between 5°N and 10°S during boreal spring, visible on the zonal mean of the SST, WV and wind speed (Figure 1(b)–(d)): north of the equator, characterized by the wettest atmosphere and the warmest SST; south of the equator, less wet and with the coldest SST; and a drier southern zone with a slightly warmer SST. The wind follows a similar scheme: maximum north (> 6.5 m s^{-1}), strongly decreasing south of the equator (about 5.5 m s^{-1}), and then strengthening again in the Southern Atlantic (> 6 m s^{-1}; Figure 1(d)). The WV increases linearly from south to north (Figure 1(c)). These three areas were therefore delimited for the study, as in Marin *et al.* (2009): the North Area from 4.5°N to 1°N, the Upwelling Area from 1°N to 4°S and the South Area from 4°S to 8°S (grey frames in Figure 1(a)). These areas were taken between 10°W and 6°E in longitude, far from the African coastline and islands.

Figure 3 shows the TMI and QuikScat measurements averaged in each area from April to July 2006. At first sight, a decrease of 5–6°C over the whole period is generally observed in the SST, as well as a WV decrease of about 15 kg m^{-2}. In agreement with Figure 1(d), the WV exhibits a sharp

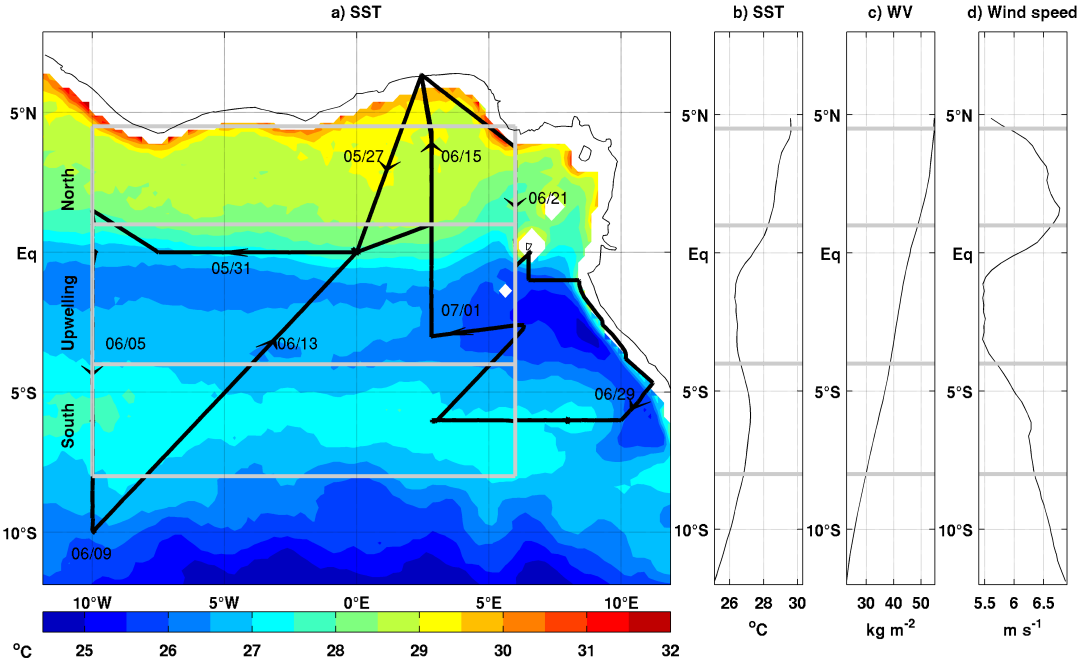

Figure 1. (a) Map of the mean SST TMI between 15 May and 15 June 2006. The trackline of the EGEE cruise in May-July 2006 in the Gulf of Guinea is superimposed. (b–d) Meridional section averaged between 12°W and 12°E of SST TMI (b), WV TMI (c) and wind speed QuikScat (d). The grey lines define the various areas of the Gulf.

Table 1. Mean and standard deviation (STD) of SST and WV for in situ, satellite and operational analyses data.[a]

	SST (°C)			WV (kg m^{-2})		
	EGEE	TMI	ECMWF	EGEE	TMI	ECMWF
Mean	26.88	26.65	26.76	45.1	40.0	41.9
STD	1.38	1.22	1.31	12.5	9.6	11.3
Mean diff.	–	-0.01	-0.13	–	-3.2	-3.8
STD diff.	–	0.50	0.54	–	4.1	2.1

[a]Difference between in situ data used as reference and satellite data and operational analyses.

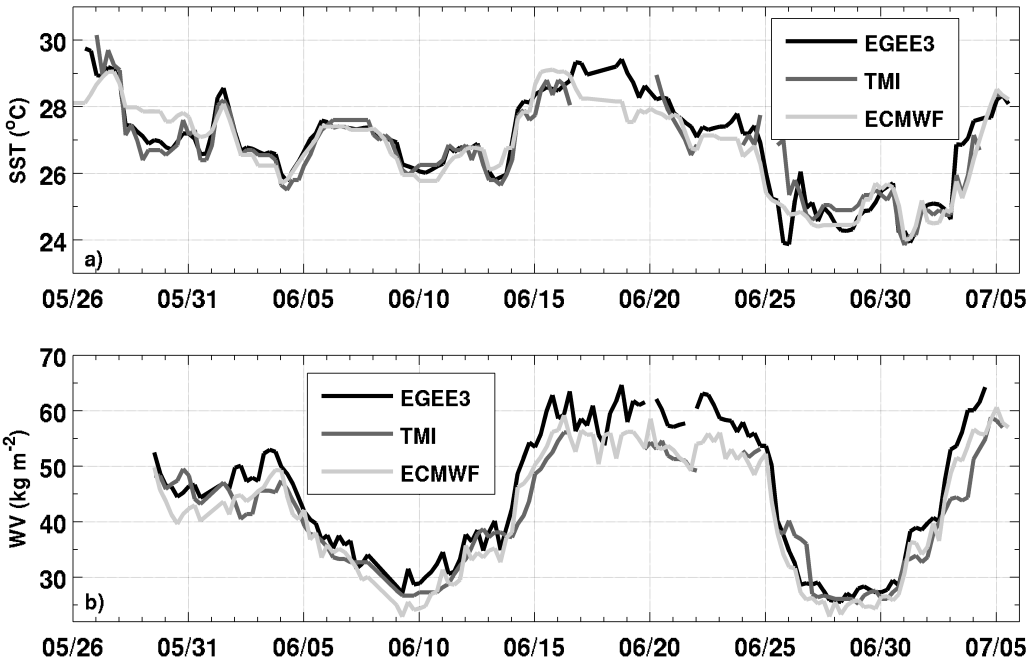

Figure 2. Hourly mean SST (a) and WV (b) during the EGEE cruise from 27 May to 5 July 2006. TMI satellite and ECMWF operational analyses of 0.25° resolution at the closest grid point and time from the ship location.

south–north gradient from April to July 2006, with the humidity maximum standing in the North Area. Southeasterlies in the South Area become southsouthwesterlies in the North Area after crossing the equator, due to the Coriolis effect, turning from a leftward deflection of the wind into a rightward deviation.

The Upwelling Area is marked by the most intense SST cooling between April and July (of 6.4°C). This cooling is not smooth and continuous, but results from the succession of events of various durations. As the cooling is less important in the South Area, the SST is globally 0.5°C warmer than in the Upwelling Area. Moreover, the mean surface wind in the South Area weakens from about 7 m s^{-1} to less than 6 m s^{-1} in the Upwelling Area. In both areas, the surface wind tends to weaken after the end of June.

A similar comparison shows that the mean SST from April to July in the North Area is 2.4°C warmer than in the Upwelling Area. This meridional SST gradient between the equator and 1°N is stronger in July (with a mean difference between the two areas of about 3°C) than in April (about 1.8°C). In April, the surface wind is quite weak (less than 5 m s^{-1}) in the North Area, but strengthens from May to July to reach 6.9 m s^{-1} (against 5.4 m s^{-1} in the Upwelling Area). In parallel, whereas the Upwelling Area sky is mainly clear, theNorth Area has an overcast sky with the presence of some high clouds (MSG classification, Derrien and Le Gléau (2005), not shown). Thus a strong intraseasonal variability in the SST, wind speed and WV is exhibited in Figure 3.

A wavelet analysis was performed on the parameters in the three areas and revealed three main modes (Figure 4). In each area, the WV variability is dominated by a 40–day periodicity. Time series spanning over 4 months are too short to statistically confirm a mode with a 40–day periodicity here, but at least this agrees with Eymard *et al.* (2010), who also found an intraseasonal 30– to 40–day mode between 5°W–5°E and 20°S–10°S in the 2005–2007 period, by using AMSU–B data on the humidity in the troposphere (at about 3 and 8 km of altitude). This frequency could be linked to a Madden–Julian oscillation (Matthews 2004; Janicot *et al.* 2009), or also perhaps to the Southern Hemisphere equivalent of the North Atlantic Oscillation (Foltz and McPhaden 2004). Then, a mode with periods from 15 to 20 days dominates the SST intraseasonal variability in the three areas, with the strongest domination found in the Upwelling Area. This is also observed in the wind variability in the three areas, equally, albeit less intensely. Eventually, an 8– to 10–day mode appears in the wind and WV variability for the Upwelling and South Areas. These various variability modes are discussed in section 5.3.

Altogether, this suggests that the upwelling development influences the low atmosphere circulation, spatially (since it divides the region into roughly three areas), as well as temporally. The strong meridional SST gradient between the Equator and 1°N appears to be a key zone for the air–sea interactions in the eastern equatorial Atlantic: in order to properly address the processes affecting the MABL response to this SST front, it is useful to make a clear distinction between the processes occurring on either side of the front and those occurring in the frontal region itself.

4. Impact of the SST front

4.1. Mean characteristics of the MABL on either side of the SST front

A first approach to study the link between the SST and the MABL was to compare the vertical MABL structures above the cold SST in the Upwelling Area and the warmer SST in the North Area. Figure 5 shows the mean profiles of the soundings made above the cold SST (between 0°N and 3°S) and the warmer SST (between 4.5°N and 1°N) from 2 to 5 July 2006, when the ship followed a meridional direction along 3°E. A preliminary study of the SST, wind and relative humidity variations showed that their diurnal cycle does not perturb the mean of the soundings made at different hours (not shown).

The mean potential temperature exhibits very similar profiles on both sides of the front (Figure 5(a)). Two different layers in the MABL are observed: a well–mixed layer, extending from the surface up to 500 m high, and the layer up to the MABL top, characterized by a large stability.

In the mixed layer, a nearly constant potential temperature takes place, in agreement with the existence of strong surface buoyancy fluxes near the surface (Small *et al.* 2008), a strong relative humidity (Figure 5(b)) and a maximal wind speed (Figure 5(c)). Note that the wind speed in the mixed layer is weaker (about 6.5 m s^{-1} maximum) on the cold side than above the warm SST (8 m s^{-1} maximum), in agreement with the observations made in the previous section with satellite wind data at the surface.

The location of the MABL top can be seen here in the profiles of Figure 5 as a decrease in the relative humidity, a wind speed minimum and a sharp wind shear where the wind turns westward. Significant contrasts appear between the profiles above the cold and warm sides. The MABL is wetter above the warm side: the relative humidity is of about 90 % on average in the MABL and remains important (more than 80 %) above the MABL top at the vicinity of 2000 m high. Moreover, the wind speed minimum (of 2.7 and 2.2 m s^{-1} respectively above the cold and the warm SST) stands higher on the warm side (1600 m) than on the cold side (1100 m). The same applies to the wind shear altitude. Thus, these observations show that the MABL is thicker above the warm SST than the cold SST. This agrees with the clear spatial and temporal coherence found in the previous section between the surface wind and SST patterns. Several previous studies of the SST front in the Pacific or North Atlantic also emphasized the same characteristics (Businger and Shaw 1984; Friehe *et al.* 1991; Kwon *et al.* 1998; Hashizume *et al.* 2002; Small *et al.* 2008). To obtain a wide view of the differences between both sides of the SST front, ECMWF operational analyses are used to compute the mixed layer and the MABL heights.

4.1.1. Determination of the mixed layer and MABL heights

Several methods exist to compute the MABL thickness. The cloud base was often used as a cut–off for the MABL (Kwon *et al.* 1998). Wayland and Raman (1989) and Hashizume *et al.* (2002) used virtual potential temperature profiles, searching the maximal gradient. Mathieu *et al.* (2004) computed the MABL height by using the Richardson number, but this method requires the fixing of a critical Richardson number, on

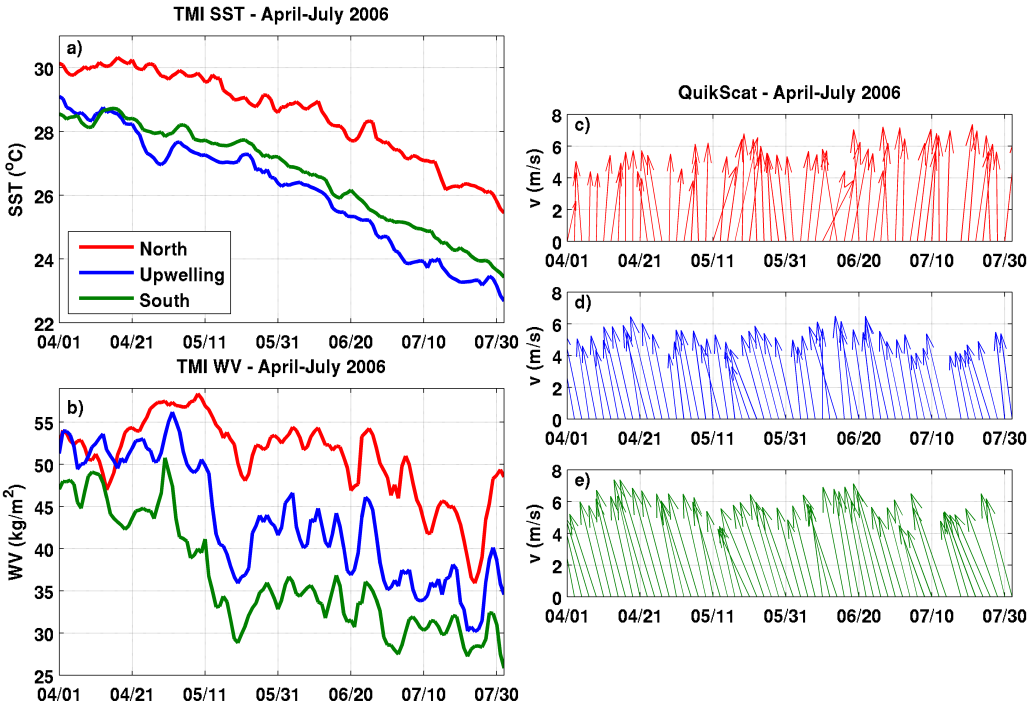

Figure 3. SST (a) and WV (b) measured by TMI and wind vector by QuikScat from May to July 2006 for North (c), Upwelling (d) and South Area (e).

which the MABL height depends strongly. This is the method used in the ECMWF analyses, but it leads generally to thinner MABL layers than those observed (Palm *et al.* 2005).

Here, the potential temperature criterion was used (note that using the virtual potential temperature instead does not change the results). As shown in the previous section, EGEE–3 soundings led to defining the MABL top as the altitude where the gradient of the potential temperature between 700 and 2500 m is maximal. The definition of the upper limit prevents the top rises up to several kilometres in the deep convection areas; the lower limit stops at the mixed layer top, which can also be characterized by a strong potential temperature gradient (Hashizume *et al.* 2002). Thus the mixed layer top can be defined as being collocated with the lowest level where the potential temperature increases by more than 0.3 K with a 100 m increase in height. In some cases, where the mixed layer is more than 700 m high, it is considered to merge with the MABL top. Moreover, a strong draining exists at the MABL top: a comparison with the specific humidity maximum gradient can be used to check the consistency of this maximum altitude with the MABL height computation. They are in very good agreement, except near the Guinean coast and in the northeastern part of the domain, where some deep atmospheric convection takes place (not shown).

4.1.2. Structure of the mixed layer and MABL

Maps of MABL and mixed layer thicknesses were computed with these criteria by using ECMWF operational analyses. In early May, when there is no SST front at the equator, no characteristic pattern is observed (not shown). As the SST front develops, however, the layer heights change. Figure 6 shows the average of the mixed layer and MABL heights in the first 10 days of July 2006, when the SST front is well established. Their thickness is clearly larger over a warmer temperature: about 1800 m for the MABL and 550 m for the mixed layer are observed on the warm side, against about 1000 m and 350 m respectively on the cold side. Moreover, the spatial fluctuations of the mixed layer height are very well collocated with the SST ones. This indicates that the mixed layer fully responds to the local SST changes through heat flux variations. The changes in MABL height due to the SST front also show very similar spatial fluctuations, albeit located downstream of the SST gradient. This difference between mixed layer and MABL is discussed in section 5.

4.2. Across the SST front

A second approach consisted of investigating the MABL during the crossing of the SST front, in particular when there is a strong cooling in the Upwelling Area. Indeed, the development of the equatorial cold tongue between April and July is not smooth and continuous. Instead, its formation results from the succession of cooling events of short or long duration (Figure 3). In parallel to these events, short or long periods of stronger wind are observed.

Figure 7 focuses on two particular sequences of 10 days each, at the end of April and June 2006, during a strong wind event (about 9 m s^{-1}) in the South Area. A strong negative SST anomaly (< –0.5°C) develops south of the equator and stretches as far as 3°S in April and 5°S at the end of June (Figure 7(a)). In both sequences, a strong wind appears in the South Area, slows down above the cold SST in the Upwelling Area and then accelerates north of the Equator. This acceleration stops around 2°N in April, but reaches 4°N at the end of June. Moreover, the surface wind is convergent north of 2°N in April (Figure 7(b)), where the WV is maximal (> 60 %), suggesting the occurrence of deep atmospheric convection there. Conversely, no convergence is observed at the end of June, when the northern part of the Gulf of Guinea is rather dry (< 55 %).

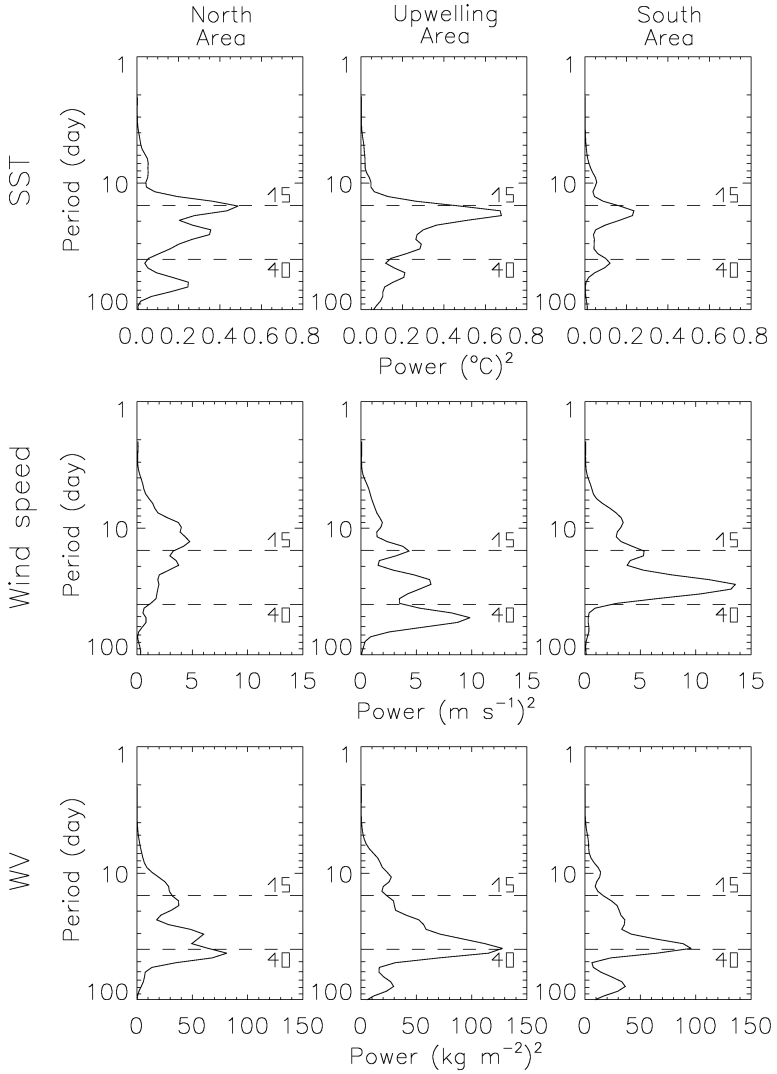

Figure 4. Mean wavelet spectrum energy for the TMI SST (top), QuikScat wind speed (center) and TMI WV (bottom) between April and July 2006 in North (right column), Upwelling (centre column) and South Area (left column). A high pass filter was applied to remove the seasonal signal.

This agrees with Janicot et al. (2008), who described an intensification of the convective activity during the second half of April and most of May 2006 off the Guinean coast, and a weakening of the convection at the end of June, as the ITCZ migrates northward. Thus, in the same way as the MABL thickness (see previous section), some differences take place depending on the period within the April–July season. However, the physical processes of the air–sea interactions remain quite similar all along the season.

In order to investigate these physical processes linking the fluctuations in the low atmosphere and the surface ocean during the successive SST coolings, composites were computed and averaged in the meridional band between 6°W and 10°W. This area was chosen because it is far from the African coastline to the East, while staying within the EGEE–3 cruise area and thus benefiting from its data assimilation in the ECMWF model. Moreover, the oceanic and atmospheric patterns are the most marked there (see, for example, Figure 1 for the SST and Figure 6 for the MABL height). The largest SST variation is located between 1°S and 3°S over the whole period. The criterion used to extract the set of dates for the composite is a SST cooling of at least 0.1°C per day in the TMI data averaged over the 6–10°W/1–3°S region. This zone between 1°S and 3°S is chosen because it is in the Upwelling Area where the cooling is the most intense and away from the transition zones between the other areas. Thirty–two days of such cooling events were found between April and July 2006 (representing about 25 % of the time period). This set was then divided into two subsets: the first one selects only short cooling events of only 1 day duration (10 events selected, case 1), and the second one selects the cooling events lasting between 2 and 5 days (22 selected, case 2). Composites on both datasets of these dates were computed using satellite data (TMI SST and WV, QuikScat wind) and the ECMWF operational analyses. Composites with temporal lags were computed, from 2 days before the cooling dates to 7 days after, showing the complete event development on a full 10–day period in both cases (short and long). Eventually, at each meridional gridpoint, the significance of the composite was tested using a Monte Carlo method: 1000 subsets of 10 days were randomly generated between April and July 2006, and the 901st value among the sorted 1000 resulting composites gave the 10 % significant threshold.

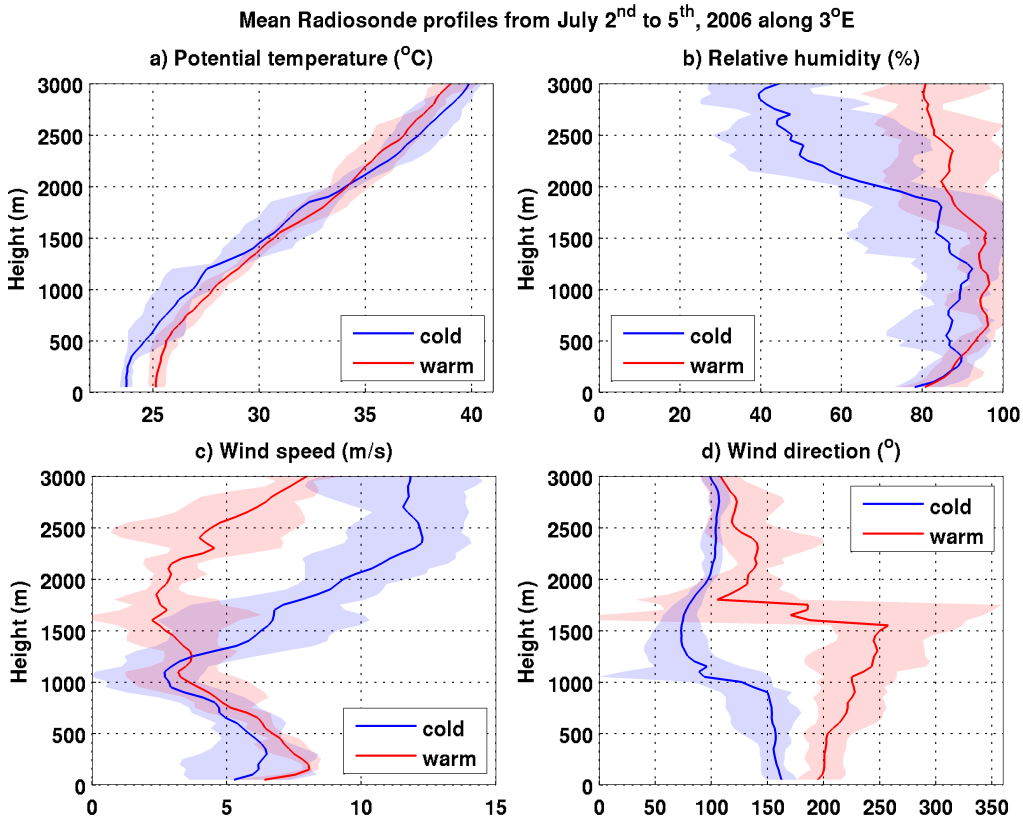

Figure 5. Mean profiles of (a) potential temperature (°C), (b) relative humidity (%), (c) wind speed (m s^{-1}) and (d) wind direction (0° northward, clockwise) over warm (plain lines) and cold sides (dashed lines) with envelope as computed by the EGEE radiosondes from 2 to 5 July 2006, along 3°E. There are 4 (5) radiosondes for the warm (cold) side.

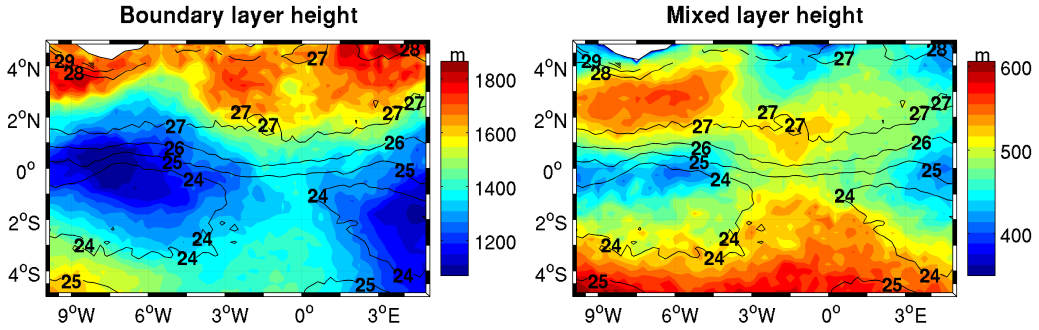

Figure 6. Boundary layer (left) and mixed layer (right) height (m, colours) computed with ECMWF operational analyses and SST TMI (°C, black contours) between 1 and 10 July 2006.

Figure 8 shows the composites of the TMI SST and the QuikScat wind speed. In case 1, in the southern part of the domain, a strong wind (> 7.5 m s^{-1}) precedes the SST cooling (lag –2 to 0) and tends to slow down afterwards (about 7 m s^{-1}). In comparison, in case 2, the wind is stronger and longer (> 8 m s^{-1}, from lag –1 to lag 3) and slows down around lag 4 (about 7.5 m s^{-1}). In both cases, between 2°S and the equator, the surface wind is clearly much weaker, both spatially and temporally, with a cooler SST in parallel: this agrees with a vertical stability in the MABL increased by a colder SST, which would limit the downward momentum flux of stronger winds aloft (as described in Wallace *et al.* (1989). North of the SST front, the wind strengthens up to 7 m s^{-1} for a period significantly longer in case 2 than in case 1 at 2°N (Figure 8). Other tests show that the patterns are generally not significant in case 1, suggesting that isolated SST cooling events are not linked to some notable change in the atmosphere.

Composites of the ECMWF operational analyses for case 2 in the three areas are shown in Figure 9. Unfortunately, this dataset is only available over a region limited to 5°S in latitude (section 2); thus the South Area is restricted here between 4°S and 5°S. The wind pattern up to about 2000 m high remains similar to the surface wind one (Figure 9(a)–(c)): the wind strengthening during the first days is indeed observed in the whole MABL, as well as its weakening above the cold SST in the Upwelling Area (at lag 4). A wind speed minimum is also reached in the North Area at lag 3. However, the wind is much slower there than in the Upwelling Area, contrary to what was observed in the composites of satellite data (Figure 8). Hersbach (2010) observed the same underestimation of the

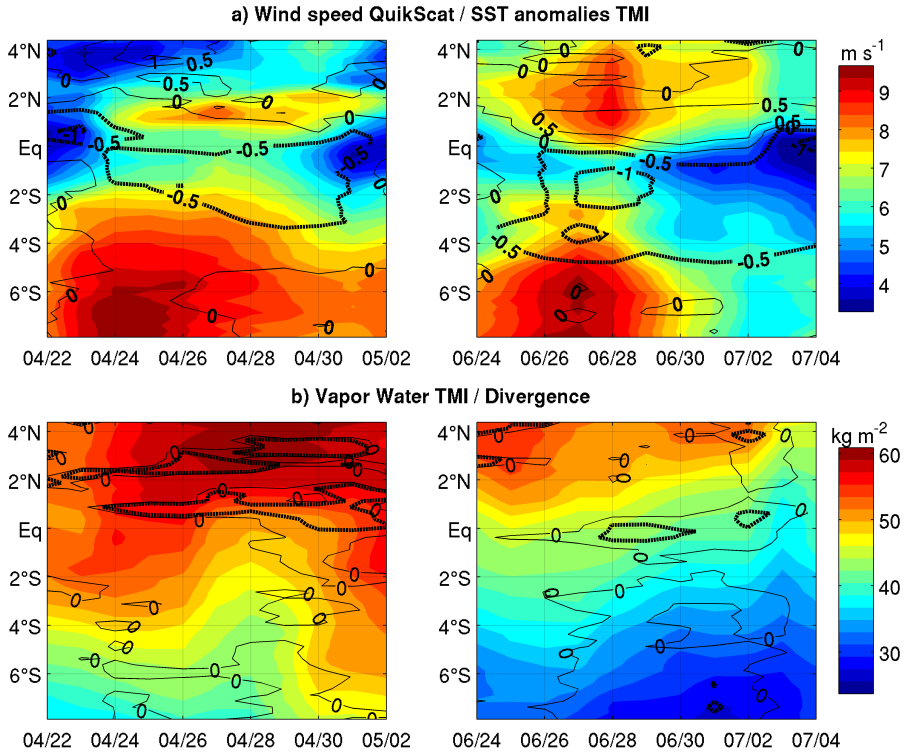

Figure 7. (a) QuikScat wind speed (colours, m s^{-1}) and TMI SST anomaly (black contours, °C) between 22 April and 2 May 2006 (right) and 24 June and 4 July 2006 (left). Anomaly is computed removing by the cubic tendency in the SST time series. (b) TMI WV (colours, kg m^{-2}) and wind divergence computed with QuikScat measurements (only two contours are plotted: plain for 0 and dotted for 1.10^{-5}, s^{-1}).

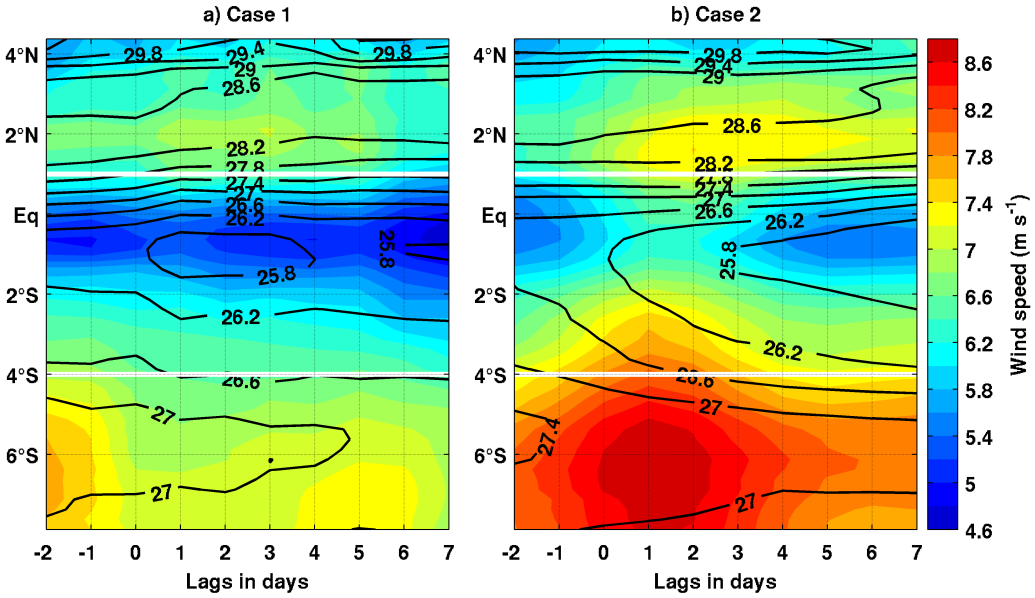

Figure 8. QuikScat wind speed (colours, m s^{-1}) and TMI SST (black contours, °C) composites for (a) case 1 and (b) case 2 (see text for details). White lines limit the various areas of the Gulf.

surface wind speed in the Gulf of Guinea by the operational ECMWF when compared with scatterometer data, and suggested it could be due to stability–dependent errors in the ECMWF boundary layer formalism. Note, however, that the wind maximum is observed at an altitude of about 500 m, in agreement with the radiosoundings shown in section 4.1.

As both relative humidity and potential temperature are continuously and strongly stratified between the surface and 3 km high (not shown), their anomalies were computed by removing the temporal cubic tendency at each gridpoint (latitude, longitude, altitude) and their composites performed on these anomalies instead of their absolute values. A strong positive anomaly of relative humidity is observed in the MABL with a maximum near the top of the MABL (about 2000 m) in the three areas around lag 3 (*i.e.* 3 days after the SST cooling, Figure 9(d)–(f)). This coincides with a strong negative anomaly of potential temperature. At this altitude, just above the top of the MABL, the winds are no more northwestward as in the

MABL, but have a strong westward component (not shown), advecting colder and wetter air from the free troposphere further east (toward the African continent), thereby creating these anomalies.

While these colder and wetter anomalies are restricted to the top of the MABL in the Upwelling and South Areas (other anomalies observed in both of these areas are generally not significant and thus will not be discussed), in the North Area, on the contrary, the relative humidity anomaly stretches significantly vertically in the whole MABL column around lag 3. The WV would thus be logically stronger than usual in the North Area from lag 1 to 5, which was indeed found in the TMI WV composites, as well as in the TMI liquid cloud water north of 2°N (not shown). Moreover, the cold anomaly of air temperature at the top of the MABL is found, as well as at its base. The presence of such a wet and cold atmosphere in the whole column in the North Area suggests an increased convective activity in the low atmosphere, a few days after the strongest wind event taking place in the southern part. This is probably linked with the signal found in the composite of the TRMM rainfall product (3b42, Huffman *et al.* (2001)), which exhibits significant precipitation at the same time north of 2°N (not shown).

5. Discussion and conclusion

5.1. The interaction between oceanic surface and atmosphere

The analysis of the 2006 boreal spring provides some information on the air–sea coupling mechanisms in the Gulf of Guinea. With a composite analysis based on the SST cooling in the Upwelling Area (section 4), it was shown that this cooling is led by an intensification of the southeasterlies in the South Area. The cooling starts immediately, and leads to a maximum SST anomaly a few days later. This agrees with de Coëtlogon *et al.* (2010), who found similar results by performing lagged linear regressions onto an intraseasonal index of the SST variability on years 2000–2007. It was proposed that the SST cooling was partly due to the horizontal advection of colder waters in the cold tongue, dragged northward by stronger than usual southerlies, and also probably to vertical mixing oceanic processes (entrainment + diffusion). The wind strongly slows down in the Upwelling Area, and strengthens in the North Area. A linking mechanism between the SST and the wind was first described by Sweet *et al.* (1981) and Wallace *et al.* (1989); the vertical stability of the atmospheric column is enhanced through decreased surface turbulent heat fluxes when passing over colder water, and this would decrease the downward vertical momentum flux coming from the stronger winds aloft (*i.e.* from the top of the atmospheric mixed layer, which is about 500 m high in this region, as shown in section 4.1.1). As the wind blows from cool to warm waters, the surface fluxes increase, the atmospheric mixed layer is destabilized, and the vertical mixing enhances, increasing the observed surface winds.

However, a decrease in the wind speed is observed not only in the surface winds but also in the whole MABL (Figure 9, left); this suggests that the mechanism could rather be linked to the dynamics of the MABL itself, and particularly to the adjustment of its height, instead of a simple shear in the sole mixed layer. This is confirmed by the very good spatial correlation obtained between the SST and the MABL height (and to a lesser extent the mixed layer height) when the latter was averaged over a 10–day period (Figure 6). These results are thus in agreement with previous studies (Sweet *et al.* 1981; Wayland and Raman 1989; Kwon *et al.* 1998; Hashizume *et al.* 2002), which discussed in particular how the adjustment of the mixed layer and the MABL to a SST front differs: the thin mixed layer responds to the local changes in the SST, whereas the thicker MABL follows the SST variations with a spatial and temporal lag, due to the advection by the mean atmospheric flow.

5.2. Role of the SST front

The SST front also has an effect on the MABL dynamics. Indeed, Small *et al.* (2008) explained that pressure anomalies are due to the change in air temperature and moisture induced by the SST front, with lower pressure over the warm air, and higher pressure over the cold air. Due to the thermal advection, the length scale of the adjustment of the whole MABL may be longer than the SST frontal width. The height of the MABL maximal gradient is hence located downstream of the SST gradient. No clear signal can be seen in the sea–level pressure composite (not shown). In the same way, no significant signal was obtained directly in the composites of the MABL height, but this probably comes from the delayed response of the MABL height to SST fluctuations. Moreover, this height is computed indirectly from the discretized model levels in the operational model, which must raise large uncertainties. However, the strong positive anomaly in the relative humidity found in the composites at the top of the MABL is an indirect proof of this influence (Figure 9, right): as most of the humidity remains within the boundary layer, by definition, a very strong vertical gradient of humidity takes place at its top; it is thus expected to produce large anomalies of humidity around the MABL top, even with weak fluctuations of its altitude (note that this could result from a local budget of humidity, as well as from the advection of some air with different temperature and humidity in the free troposphere).

Thus the cold tongue development tends to stabilize the atmosphere above the cold water, but the equatorial SST front strongly destabilizes the MABL in the northern part of the cold tongue. This suggests a link between the upwelling development and the onset of the coastal rainfall season, since the latter benefits from the increased atmospheric instability leading to the development of convective activity (Thorncroft *et al.* 2011). The presence of a strong atmospheric convergence north of 2°N in April–May 2006 (Figure 7(b)), which migrates northward in June–July, therefore suggests an influence of the upwelling on the convection. This is also emphasized by the greater cloud cover over the warm side of a SST front, which was observed here with the MSG classification in the North Area (not shown) and in other several studies (Rogers 1989; Deser *et al.* 1993; Xie 2004; Small *et al.* 2008). For example, Pyatt *et al.* (2005), who studied the structure of the MABL over an SST front in the tropical eastern Pacific Ocean, found variable cloudiness on the cold side (coverage of 20–90 %), and high cloudiness (greater than 80 %), as well as being quite constant in time, on the warm side with the highest cloud tops, which suggests deep convection. Further investigations

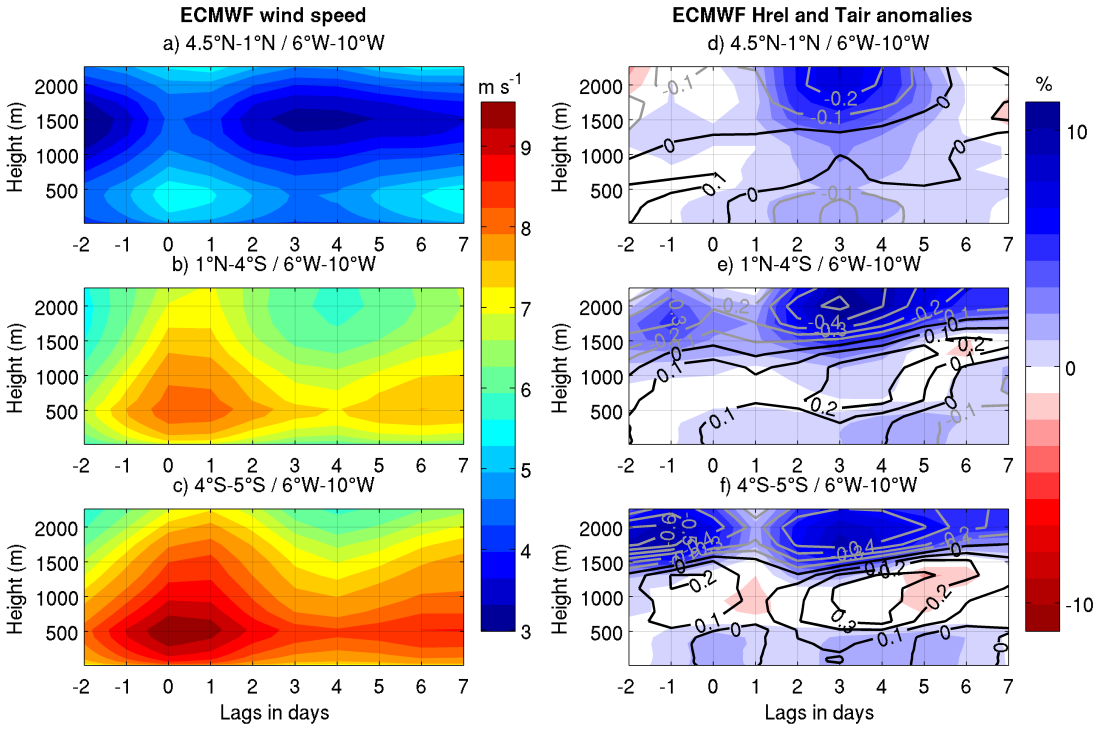

Figure 9. ECMWF operational analyses composite of (a–c) wind speed (m s^{-1}) and (d–f) relative humidity (colours, %) and air temperature (contours (grey negative and black positive), °C) anomalies for case 2 according to altitude averaged between 6°W and 10°W and in three boxes: North Area (a,d), Upwelling Area (b,e) and 4–5°S (c,f). Anomalies are computed removing the cubic tendency in the time series.

are thus needed to document the interaction between the SST front and the coastal convection.

5.3. The intraseasonal variability mechanisms

The intraseasonal variability of the SST and the surface wind was investigated using wavelet analysis (Figure 4). This showed a very robust 15– to 20–day main periodicity in both SST and wind speed. Garzoli (1987), Houghton and Colin (1987), Athié and Marin (2008) and Guiavarc'h *et al.* (2009) determined that this intraseasonal variability in the SST is rather locally forced by the 15–day variability found in the surface wind. On the other hand, Athié and Marin (2008) showed that the intensity of this signature depends strongly on the presence, and intensity, of the seasonal SST front, north of the equatorial cold tongue. The intraseasonal variability of the wind has also been linked to a zonal dipole of convection between the Guinean coast and the mid–Atlantic (Sultan *et al.* 2003; Mounier and Janicot 2004; Mounier *et al.* 2008). In addition, a large part of the wind in the Gulf of Guinea can be related to the Santa Helena anticyclone (Marin *et al.* 2009; de Coëtlogon *et al.* 2010). Although the latter does not exhibit a significant biweekly variability (de Coëtlogon *et al.* 2010), the South Atlantic variability could nonetheless explain the 8– to 10–day mode which appears in the wind and WV variability in the Upwelling and South Areas (section 3). Indeed, the composite analysis and the study of specific wind bursts in April and June (section 4) showed that some strong wind events are more effective for the SST cooling, south of the equator. In the same way, Marin *et al.* (2009) observed that the intraseasonal intensifications of the southeast trades are the major contributor to the SST cooling, but that their efficiency depends crucially upon their intensity, their equatorward extension, and the local oceanic conditions at the time of their occurrence. This can suggest that the wind bursts are possibly most effective when the 15–day wind variability in the Gulf of Guinea and the shorter one in the South Atlantic are in phase. A study of the link between these two variability modes could be interesting.

5.4. Summary and perspectives

The influence of the SST cooling on the MABL in the Gulf of Guinea from April to July 2006 was investigated using in situ measurements, satellite data and ECMWF operational analyses. A short description of the region (5°N–10°S/10°W–6°E) led to the definition of three areas, which globally become cooler and dryer during this period. The North Area (from 4.5°N to 1°N) is the warmest, wettest and cloudiest, with southerlies tending to strengthen by the end of June and turn northeastward. The Upwelling Area (from 1°N to 4°S) has the coldest SST, but the humidity remains high although drier than the North Area. The South Area (from 4°S to 8°S) is the driest, with a warmer SST than in the Upwelling Area and the strongest southeasterlies.

Strong southeast wind events in the South Area lead to SST cooling steps in the Upwelling Area, where the wind weakens. This cooling creates a strong gradient of SST between Upwelling and North Areas, which appears to be a key zone for the air–sea interactions in the eastern equatorial Atlantic. A thickening of the MABL and an acceleration of the wind are then observed in the North Area. In addition, in the same area, the increasing humidity in the atmosphere and the convergence zone of the surface wind suggest a convection activity, which can contribute to the onset of the rainfall season on the West African coast. Moreover, a 15–day variability

mode would link the wind and the SST, and an 8– to 10–day mode would link the wind to the variability in the South Atlantic.

A study over several years needs to be conducted to test the validity of the mechanisms observed in 2006. Owing to the prominent role that they could play in the region, particularly on the coastal monsoon onset as discussed previously, a thorough investigation is strongly needed here, for example with regional modelling allowing the study of small–scale features in the atmospheric circulation. It would also be interesting to extend the study to the African coastal region and to the free troposphere in order to understand the mechanisms linking the SST in the Gulf of Guinea and the precipitation in West African. For example, the African easterly jet, located around 5–10°N at about 600 hPa, was stronger than usual from June to August 2006, which could be explained by the enhanced convection observed here near the coast (Janicot *et al.* 2008). Finally, an in–depth study of the intraseasonal variability must be made to emphasize the leading modes in the different parameters, as well as the mechanisms linked to their interaction.

Acknowledgements

Based on a French initiative, AMMA was built by an international scientific group and is currently funded by a large number of agencies, including those in France, the UK, USA and Africa. It has been the beneficiary of a major financial contribution from the European Community's Sixth Framework Research Programme. Detailed information on scientific coordination and funding is available on the AMMA International website: http://www.amma-international.org. TMI data are sponsored by the NASA Earth Science MEaSUREs DISCOVER Project and QuikScat data by the NASA Ocean Vector Winds Science Team. They are produced by Remote Sensing Systems and are available at www.remss.com. The authors wish to thank G. Caniaux, S. Janicot and A. Weill for their help, as well as the reviewers for their constructive remarks.

References

Athié G, Marin F. 2008. Cross-equatorial structure and temporal modulation of intraseasonal variability at the surface of the tropical Atlantic ocean. *J. Geophys. Res.* **113**(C8), doi:10.1029/2007JC004332.

Bourlès B, Brandt P, Caniaux G, Dengler M, Gouriou Y, Key E, Lumpkin R, Marin F, Molinari RL, Schmid C. 2007. African monsoon multidisciplinary analysis (AMMA): Special measurements in the tropical Atlantic. *CLIVAR Exchanges* **12**(2): 7–9.

Businger JA, Shaw WJ. 1984. The response of the marine boundary layer to mesoscale variations in sea-surface temperature. *Dyn. Atm. Oceans* **8**(3-4): 267–281, doi:10.1016/0377-0265(84)90012-5.

Caniaux G, Giordani H, Redelsperger JL, Guichard F, Key E, Wade M. 2011. Coupling between the Atlantic cold tongue and the west african monsoon in boreal spring and summer. *J. Geophys. Res.* **116**(C04003), doi: 10.1029/2010JC006570.

de Coëtlogon G, Janicot S, Lazar A. 2010. Intraseasonal variability of the ocean - atmosphere coupling in the Gulf of Guinea during boreal spring and summer. *Q. J. R. Meteorol. Soc.* **136**(Sp. Iss. SI Suppl. 1): 426–441, doi: 10.1002/qj.554.

Derrien M, Le Gléau H. 2005. MSG/SEVIRI cloud mask and type from SAFNWC. *Int. J. Remote Sens.* **26**(21): 4707 – 4732, doi: 10.1080/01431160500166128.

Deser C, Wahl S, Bates JJ. 1993. The Influence of sea surface temperature gradients on stratiform cloudiness along the equatorial front in the pacific ocean. *J. Clim.* **6**(6): 1172–1180.

Eymard L, Karbou F, Janicot S, Chouaib N, Pinsard F. 2010. On the use of advanced microwave sounding unit-a and-b measurements for studying the monsoon variability over west africa. *J. Geophys. Res.* **115**(D20): D20 115, doi:10.1029/2009JD012935.

Eymard L, Planton S, Durand P, LeVisage C, LeTraon P, Prieur L, Weill A, Hauser D, Rolland J, Pelon J, Baudin F, Benech B, Brenguier J, Caniaux G, DeMey P, Dombrowski E, Druilhet A, Dupuis H, Ferret B, Flamant C, Flamant P, Hernandez F, Jourdan D, Katsaros K, Lambert D, Lefèvre J, LeBorgne P, LeSquere B, Marsoin A, Roquet H, Tournadre J, Trouillet V, Tychensky A, Zakardjian B. 1996. Study of the air-sea interactions at the mesoscale: The SEMAPHORE experiment. *Ann. Geophys.* **14**(9): 986–1015.

Fleury L, Boichard JL, Brissebrat G, Cloché S, Eymard L, Mastrorillo L, Moulaye O, Ramage K, Asencio N, Coppeaux J, Devic MP, Favot F, Ginoux K, Lafore JP, Polcher J, Redelsperger JL, Roussot O, Tytéca M. 2011. Amma information system: an efficient cross-disciplinary tool and a legacy for forthcoming projects. *Atmospheric Science Letters* **12**(1): 149–154, doi: 10.1002/asl.303, URL `http://dx.doi.org/10.1002/asl.303`.

Foltz GR, McPhaden MJ. 2004. The 30-70 day oscillations in the tropical Atlantic. *Geophys. Res. Lett.* **31**(15), doi:10.1029/2004GL020023.

Friehe CA, Shaw WJ, Rogers DP, Davidson KL, Large WG, Stage SA, Crescenti GH, Khalsa SJS, Greenhut GK, Li F. 1991. Air-sea fluxes and surface layer turbulence around a sea surface temperature front. *J. Geophys. Res.* **96**(C5): 8593–8609.

Garzoli SL. 1987. Forced-oscillations on the equatorial Atlantic basin during the seasonal response of the equatorial Atlantic program (1983-1984). *J. Geophys. Res.* **92**(C5): 5089–5100.

Gu G, Adler R. 2004. Seasonal evolution and variability associated with the west african monsoon system. *J. Clim.* **17**(17): 3364–3377, doi: 10.1175/1520-0442(2004)017<3364:SEAVAW>2.0.CO;2.

Guiavarc'h C, Tréguier AM, Vangriesheim A. 2009. Deep currents in the Gulf of Guinea: along slope propagation of intraseasonal waves. *Ocean Science* **5**(2): 141–153, doi:10.5194/osd-6-57-2009.

Hashizume H, Xie SP, Fujiwara M, Shiotani M, Watanabe T, Tanimoto Y, Liu WT, Takeuchi K. 2002. Direct observations of atmospheric boundary layer response to sst variations associated with tropical Instability waves over the eastern equatorial pacific. *J. Clim.* **15**(23): 3379–3393, doi:10.1175/1520-0442(2002)015.

Hersbach H. 2010. Comparison of c-band scatterometer cmod5. n equivalent neutral winds with ecmwf. *J. Atmos. Oceanic Technol.* **27**(4): 721–736, doi: 10.1175/2009JTECHO698.1.

Houghton RW, Colin C. 1987. Wind-driven meridional eddy heat-flux in the Gulf of Guinea. *J. Geophys. Res.* **92**(C10): 10 777–10 786.

Huffman GJ, Adler RF, Morrissey MM, Bolvin DT, Curtis S, Joyce R, McGavock B, Susskind J. 2001. Global precipitation at one-degree daily resolution from multisatellite observations. *J. Hydrometeor* **2**(1): 36–50.

Janicot S, Mounier F, Hall NMJ, Leroux S, Sultan B, Kiladis GN. 2009. Dynamics of the west african monsoon. Part Iv: Analysis of 25-90-day variability of convection and the role of the Indian monsoon. *J. Clim.* **22**(6): 1541–1565, doi:10.1175/2008JCLI2314.1.

Janicot S, Thorncroft CD, Ali A, Asencio N, Berry G, Bock O, Bourlès B, Caniaux G, Chauvin F, Deme A, Kergoat L, Lafore JP, Lavaysse C, Lebel T, Marticorena B, Mounier F, Nedelec P, Redelsperger JL, Ravegnani F, Reeves CE, Roca R, de Rosnay P, Schlager H, Sultan B, Tomasini M, Ulanovsky A, ACMAD Forecasters Team. 2008. Large-scale overview of the summer monsoon over west africa during the AMMA field experiment in 2006. *Ann. Geophys.* **26**(9): 2569–2595.

Kolodziejczyk N, Bourlès B, Marin F, Grelet J, Chuchla R. 2009. Seasonal variability of the equatorial undercurrent at 10°W as inferred from recent in situ observations. *J. Geophys. Res.* **114**(C6): C06 014.

Kwon B, Benech B, Lambert D, Durand P, Druilhet A, Giordani H, Planton S. 1998. Structure of the marine atmospheric boundary layer over an oceanic thermal front: SEMAPHORE experiment. *J. Geophys. Res.* **103**(C11): 25 159–25 180.

Liu WT, Xie X, Polito PS, Xie SP, Hashizume H. 2000. Atmospheric manifestation of tropical instability wave observed by quikscat and tropical rain measuring mission. *Geophys. Res. Lett.* **27**(16): 2545–2548, doi: 10.1029/2000GL011545.

Marin F, Caniaux G, Bourlès B, Giordani H, Gouriou Y, Key E. 2009. Why were sea surface temperatures so different in the eastern equatorial Atlantic in june 2005 and 2006? *J. Phys. Oceanogr.* **39**(6): 1416–1431, doi: 10.1175/2008JPO4030.1.

Mathieu A, Lahellec A, Weill A. 2004. Evaluation of a numerical weather forecast model using boundary layer cloud-top temperature retrieved from AVHRR. *Monthly weather review* **132**(4): 915–928.

Matthews A. 2004. Intraseasonal variability over tropical africa during northern summer. *J. Clim.* **17**(12): 2427–2440.

Merle J, Fieux M, Hisard P. 1980. Annual signal and interannual anomalies of sea surface temperature in the eastern equatorial Atlantic ocean. *Deep-Sea Res.* **26**: 77–102.

Mounier F, Janicot S. 2004. Evidence of two independent modes of convection at intraseasonal timescale in the west african summer monsoon. *Geophys. Res. Lett.* **31**(16), doi:10.1029/2004GL020665.

Mounier F, Janicot S, Kiladis G. 2008. The west african monsoon dynamics. part iii: The quasi-biweekly zonal dipole. *Journal of Climate* **21**: 1911–1928, doi:10.1175/2007JCLI1706.1.

Okumura Y, Xie S. 2004. Interaction of the Atlantic equatorial cold tongue and the african monsoon. *J. Clim.* **17**(18): 3589–3602.

Palm S, Benedetti A, Spinhirne J. 2005. Validation of ecmwf global forecast model parameters using glas atmospheric channel measurements. *Geophys. Res. Lett.* **32**(22), doi:10.1029/2005GL023535.

Picaut J. 1983. Propagation of the seasonal upwelling in the eastern equatorial Atlantic. *J. Phys. Oceanogr.* **13**(1): 18–37.

Pollard RT, Guymer TH, Taylor PK. 1983. Summary of the JASIN 1978 field experiment. *Phil. Trans. R. Soc. Lond. A* **308**(1503): 221–230.

Pyatt HE, Albrecht BA, Fairall C, Hare J Eand Bond N, Minnis P, Ayers JK. 2005. Evolution of marine atmospheric boundary layer structure across the cold tongue-Itcz complex. *J. Clim.* **18**(5): 737–753, doi:10.1175/JCLI-3287.1.

Redelsperger JL, Thorncroft CD, Diedhiou A, Lebel T, Parker DJ, Polcher J. 2006. African monsoon multidisciplinary analysis - an international research project and field campaign. *Bull. Am. Meteorol. Soc.* **87**(12): 1739–1746, doi:10.1175/BAMS-87-12-1739.

Rogers DP. 1989. The marine boundary layer in the vicinity of an ocean front. *J. Atmos. Sci.* **46**(13): 2044–2062.

Small RJ, deSzoeke SP, Xie SP, O'Neill L, Seo H, Song Q, Cornillon P, Spall M, Minobe S. 2008. Air sea interaction over ocean fronts and eddies. *Dyn. Atm. Oceans* **45**(3-4): 274–319, doi:10.1016/j.dynatmoce.2008.01.001.

Stage SA, Weller RA. 1985. The frontal air-sea interaction experiment (fasInex) .1. background and scientific objectives. *Bull. Am. Meteorol. Soc.* **66**(12): 1511–1520.

Sultan B, Janicot S. 2003. The west african monsoon dynamics. Part II: The "preonset" and "onset" of the summer monsoon. *J. Clim.* **16**(21): 3407–3427.

Sultan B, Janicot S, Diedhiou A. 2003. The west african monsoon dynamics. Part I: Documentation of intraseasonal variability. *J. Clim.* **16**(21): 3389–3406.

Sweet W, Fett R, Kerling J, La Violette P. 1981. Air-sea Interaction effects in the lower troposphere across the north wall of the gulf stream. *Mon. Wea. Rev.* **109**(5): 1042–1052.

Thorncroft CD, Nguyen H, Zhang C, Peyrille P. 2011. Annual cycle of the west african monsoon: Regional circulations and associated water vapour transport. *Q. J. R. Meteorol. Soc.* **137**: 129–147, doi:10.1002/qj.728.

Vizy E, Cook K. 2001. Mechanisms by which Gulf of Guinea and eastern north Atlantic sea surface temperature anomalies can influence african rainfall. *J. Clim.* **14**(5): 795–821.

Vizy E, Cook K. 2002. Development and application of a mesoscale climate model for the tropics: Influence of sea surface temperature anomalies on the west african monsoon. *J. Geophys. Res.* **107**(D3), doi: 10.1029/2001JD000686.

Wade M, Caniaux G, duPenhoat Y, Dengler M, Giordani H, Hummels R. 2010. A one-dimensional modeling study of the diurnal cycle in the equatorial Atlantic at the pIrata buoys during the EGEE-3 campaign. *Ocean Dynamics* **61**: 1–20, doi:10.1007/s10236-010-0337-8.

Wallace JM, Mitchell TP, Deser C. 1989. The influence of sea-surface temperature on surface wind in the eastern equatorial pacific: seasonal and interannual variability. *J. Clim.* **2**(12): 1492–1499.

Wayland RJ, Raman S. 1989. Mean and turbulent structure of a baroclinic marine boundary layer during the 28 january 1986 cold-air outbreak (gale-86). *Bound.-Layer Meteor.* **48**(3): 227–254.

Wentz FJ. 1997. A well-calibrated ocean algorithm for special sensor microwave / imager. *J. Geophys. Res.* **102**(C4): 8703–8718, doi: 10.1029/96JC01751.

Wentz FJ, Gentemann C, Smith D, Chelton D. 2000. Satellite measurements of sea surface temperature through clouds. *Science* **288**(5467): 847 – 850, doi:10.1126/science.288.5467.847.

Xie SP. 2004. Satellite observations of cool ocean-atmosphere interaction. *Bull. Am. Meteorol. Soc.* **85**(2): 195–208.